ORIGINAL RESEARCH

Health Science Reports _Open Access_ WILEY

Design matters: A comparison of natural versus synthetic skin substitutes across benchtop and porcine wound healing metrics: An experimental study

Victoria L. Stefanelli | Benjamin Mintz | Ankur Gandhi | Jason Smith [ORCID]

Exploratory R&D, Integra LifeSciences, Princeton, New Jersey, USA

Correspondence
Jason Smith, Integra LifeSciences, 1100 Campus Road, Princeton, NJ 08540, USA.
Email: jason.smith@integralife.com

Abstract

Background and Aims: Skin substitutes, essential tools for helping close full thickness wounds with minimal scarring, are available in both collagen-based and synthetic polyurethane constructions. Here we explore fundamental differences between two frequently used skin substitutes and discuss how these differences may impact in vivo performance.

Methods: Polyurethane- and collagen-based matrices were characterized in vitro for pore size via scanning electron microscopy, hydrophobicity via liquid contact angle, conformability via bending angle, and biocompatibility via fibroblast and keratinocyte adhesion and proliferation. These matrices were then evaluated in a full-thickness excisional pig wound study followed by histological analysis. Statistical analysis was performed using t-tests or one-way analysis of variances with Tukey's multiple post hoc comparisons, where appropriate.

Results: Average pore diameter in the tested polyurethane matrix was over four times larger than that of the collagen matrix ($589 \pm 297\,\mu m$ vs. $132 \pm 91\,\mu m$). Through liquid contact angle measurement, the collagen matrix (not measurable) was found to be hydrophilic compared to the hydrophobic polyurethane matrix ($>90°$). The collagen matrix was significantly more conformable than the polyurethane matrix ($9 \pm 2°$ vs. $84 \pm 5°$ bending angle, respectively). Fibroblast and keratinocyte adhesion and proliferation assays elucidated a significantly greater ability of both cell types to attach and proliferate on collagen versus polyurethane. While the porcine study showed minimal contraction of either matrix material, histological findings between the two treatments were markedly different. Collagen matrices were associated with early fibroblast infiltration and fibroplasia, whereas polyurethane matrices elicited a strong multinucleated giant cell response and produced a network of comparatively aligned collagen fibrils.

Conclusions: The more favorable in vitro properties of the collagen matrix led to less inflammation and better overall tissue response in vivo. Overall, our findings

demonstrate how the choice of biomaterial and its design directly translate to differing in vivo mechanisms of action and overall tissue quality.

1 | INTRODUCTION

While wound healing is a highly conserved and efficient evolutionary process, it is innately limited, particularly with deep wounds.[1] Clinically, large surface-area burns and traumatic wounds, if left untreated, put patients at significant risk for infection and dehydration during wound healing due to a lack of epithelium. Such wounds tend to resolve primarily via contracture resulting in extensive scar formation. Skin substitutes, designed to modulate this process, emerged as a new standard of treatment for these wounds beginning in 1996 with the Food and Drug Administration approval of collagen-based Integra® Dermal Regeneration Template (IDRT) for regeneration of full-thickness dermal tissue. Widespread adoption of this technology and others aimed at addressing the same challenges is correlated with the reduction of large TBSA burn mortality and length of hospital stay.[2,3]

Conventional skin substitutes, like IDRT, consist of biologically-derived components—notably collagen and chondroitin sulfate—whose biochemical composition and physical architecture mimic that of the natural mammalian cellular environment and readily interact with host biology. These skin substitutes are eventually resorbed and remodeled at a rate commensurate with that of cell infiltration and new tissue deposition. Recently, synthetic polyurethane matrices with degradation rates tuned by hydrolytic chemistry have shown efficacy in closing wounds in both animal models[4–7] and human case studies[8,9] through mechanisms that are fundamentally different than biologically-derived skin substitutes. Designers of these matrices assert that chemical composition is of lesser importance than matrix architecture.[10]

We contend that both the chemical makeup and physical architecture of a skin substitute are integral to clinical performance with implications for both the process of wound healing and the ultimate quality of healed tissue. This hypothesis is leveraged from decades of existing research (e.g.,[11–14]) on multiple parameters of matrix design—e.g., pore size, stiffness, fiber alignment, and material composition. Here, we directly compare a natural wound healing matrix derived from collagen and chondroitin-6-sulfate (CG) to a hydrolytically biodegradable temporizing matrix (BTM) composed of polyurethane through a range of benchtop physical and biological evaluations. Benchtop results are then translated into a full-thickness porcine wound healing model complete with histologic assessment at timepoints deemed biologically appropriate for each matrix based on previous porcine in vivo data: day 9

for CG (in-house data) and day 9 and day 21 for BTM-treated[4,15,16] wounds, respectively.

Of note, several recent studies have attempted to make head-to-head comparisons of these materials in mouse,[6] sheep,[7] and pig[4] studies, using gross metrics like rate of wound healing and overall contracture at specific (and notably identical) timepoints to conclude that the synthetic matrix performs similarly to its natural counterpart. This present work aims to take a more comprehensive look at the functionality of the two matrices comparing such qualities as cell-matrix interactions, biochemistry, and the overall quality of healed tissue. We will then discuss the implications of these differences in human clinical applications.

2 | MATERIALS AND METHODS

2.1 | Materials

The skin substitutes investigated in this work consisted of collagen-chondroitin-6-sulfate matrix (CG) (Integra® Dermal Regeneration Template, IDRT, Integra LifeSciences) and polyurethane BTM (NovoSorb® BTM, Polynovo Biomaterials Pty Ltd.). For in vitro cellular experiments TenoGlide® Tendon Protector Sheet (Integra LifeSciences), a material identical to IDRT but lacks the presence of silicone, was utilized.

2.2 | Pore size measurements

All samples were cut in cross-section with a razor blade and prepared using standard methods for environmental scanning electron micrograph (SEM) (FEI Quanta 250 SEM/ESEM with Peltier cooling stage). A total of five and eight samples were studied for BTM and CG, respectively. Samples were imaged with an accelerating voltage of 5–10 kV and working distance of 10 mm at ×50 magnification. Settings were chosen to limit depth of field by encouraging signal attenuation past the working distance. This acquisition method enables visualization of in-plane features at the site of the cut via higher signal intensity relative to features further from the working distance.

Pore size for CG was calculated via thresholding in ImageJ (NIH) image analysis software where out-of-plane detail was excluded from calculation such that only pores open to the cut surface were used in

analysis. A manual review was conducted following thresholding to ensure proper demarcation between adjacent pores. Due to the increase in pore size and regular circular pore structure relative to CG, pore size calculation for BTM was conducted by thresholding following manual application of fit ellipses over individual pores. Resulting calculations for both methods were performed via discrete area measurement for each individual pore.

2.3 | Liquid contact angle evaluation

A 50 µL droplet of either deionized water, phosphate buffered saline (PBS, Corning), or citrated whole human blood (Lampire Biological Laboratories) was pipetted on top of matrix samples and allowed to equilibrate for 20 s. Images of the final droplet position were taken with an iPhone 10 camera, and Photo Protractor v2.6 was used to analyze the internal contact angle of the droplets. Angular measurements resulting in values >90 degrees are indicative of hydrophobic materials, and values <90 degrees indicate hydrophilic materials. Six droplets of each fluid type were tested on both BTM and CG samples.

2.4 | Bending angle analysis

To determine matrix conformability, materials were precut into 5 cm long by 0.5 cm wide strips and then prewetted for 10 min in PBS solution. Bending angle testing consisted of draping the matrix strip symmetrically around a 3.12 mm metal hexagonal bar, matrix side facing down (i.e., in contact with the bar), allowing a minimum of 20 s for the material to settle, and capturing the shape via photography as well as caliper measurements of the distance between the two ends of the matrix strips. Three strips of each material were tested.

2.5 | Cell adhesion and proliferation

Matrix samples were cut into 6 mm disks via biopsy punch (Miltex) and preincubated in cell-appropriate basal media and growth kit supplements (ATCC). Cells were seeded at concentrations of 9000 human dermal fibroblasts (ATCC) per well or 12,000 human keratinocytes (ATCC) per well of a nontissue culture 96-well plate ($N = 3$ per matrix type per timepoint). An additional two samples per matrix type were identically prepared with appropriate media but with no cell seeding, for use as background controls. Multiple 96-well plates were set up in this identical manner for analysis at the following timepoints: 15 min, 2, 24, 48, 72, 96 h, and 7 days. Plates were then incubated at 37°C with 5% CO_2 and 20% humidity, along with gentle orbital shaking for the first 24 h. At the appropriate timepoints, matrices were rinsed three times in basal culture media to remove any nonadherent cells and then placed in a fresh plate along with MTS dye in fresh cell media. The dye was incubated for 60 min before reading at 490 nm with background subtraction at 650 nm.

Colorimetric measurements were obtained for both sample solutions alone and sample solutions with the matrices still in the wells.

2.6 | Porcine full-thickness wound healing study and histology

A total of 32 full-thickness excisional wounds were studied across two Yorkshire pigs (35 ± 10 kg) in accordance with AAALAC and IACUC standards (Bridge PTS, IACUC protocol 21-02). Porcine dorsum was prepared for wounding via hair removal with clippers, followed by razor and shaving cream. Dorsum was rubbed with chlorhexidine and isopropyl alcohol before wounding. Wounds (3×3 cm) were created using scalpel and forceps. Hemostasis following wounding was achieved via application of gauze wetted with dilute epinephrine. CG and BTM test materials were cut to size, placed in the wounds, and sutured to the wound bed at each of the four corners. Experimental groups included CG-treated wounds ($N = 12$), BTM-treated wounds ($N = 16$), and empty/no treatment wounds ($N = 4$) and were evenly divided across both pigs with placements chosen to maintain similarity with respect to distance from the spine as well as the head. All wounds were covered with Telfa™ Clear (Cardinal Health) and then a tri-layer bolster consisting of moistened Optifoam® (Medline) cut to the wound bed size, two pieces of moistened sterile gauze, and a final moistened Optifoam bolster cut oversize. These tri-layer bolsters were secured with tie-over sutures and further covered with an absorbent pad, which was in turn held in place with ELASTIKON Elastic Tape (Medline). The dressing protocol ensured that all matrices were in intimate contact with the wound bed. Pain management after wounding was achieved with Buprenorphine HCl (0.02 mg/kg, IM) at day 0 along with a Fentanyl patch (50 µg/h, Lohmann Therapy Systems Corp.), which was replaced at appropriate intervals. Dressings were changed every 3–5 days. Tri-layer bolsters were replaced with a single-layer Optifoam "light" bolster on day 7.

On day 9 postinjury, all CG wounds ($N = 12$), half of all empty wounds ($N = 2$), and half of all BTM wounds ($N = 8$) were extracted for histological analysis. Day 9 was chosen as the primary termination point owing to our previous experience with CG matrices being ready to graft in full-thickness porcine wound models between 8 and 10 days (unpublished). The remainder of empty and BTM-treated wounds continued through day 21 at which point they were excised as well. The longer timepoint for BTM was selected in an effort to achieve wound healing more similar in duration to existing porcine wound studies utilizing BTM.[4,15,16] Extracted wound tissue was fixed in 10% neutral buffered formalin until ready for paraffin processing. Histologic analysis consisted of hematoxylin and eosin as well as Martius Scarlet Blue stain.

2.7 | Statistical analysis

Statistical analysis was performed in GraphPad Prism (GraphPad Software) using t-tests or one-way analysis of variances with Tukey's multiple post hoc comparisons, where appropriate. Each dataset was tested for normality using the Shapiro–Wilk test.

3 | RESULTS

3.1 | Pore size

BTM pores (589 ± 297 μm) were significantly larger ($p < 0.0001$, Mann–Whitney test) than those of the CG matrices (132 ± 91 μm). This was quite different from a prior study, which measured the BTM's pore size as ranging from 100 μm up to a maximum of 500 μm.[4] In contrast, we found that over 60% of BTM pores possessed diameters over 500 μm. Representative SEM images are shown in Figure 1A–C for visual analysis of the pore architecture. A histogram of the full distribution of pore sizes is shown in Figure 1D. The distribution of pore sizes was also more varied for BTM with an interquartile range extending from 385 to 771 μm compared to 68–170 μm for CG. Kurtosis of pore distribution for the materials was −0.2 and 21.2 for BTM and CG, respectively, indicating that pores in BTM take on a relatively flat distribution whereas those in CG are more tightly clustered, or peaked.

3.2 | Liquid contact angle evaluation

Droplets of all fluid types on BTM matrices beaded up, producing internal contact angles averaging 101.6 ± 6.4, 95.3 ± 9.8, and 121.1 ± 8.6 degrees, respectively, with PBS, water, and blood, all of which represent hydrophobic material behavior (Figure 2A–D). Fluid droplets on CG matrix immediately absorbed into and dispersed throughout the material, resulting in no visual droplet on the surface. As a result, droplet contact angles were not measurable for this material.

3.3 | Bending angle analysis

CG exhibited the lowest internal bending angle of 9 ± 1.5 degrees which was significantly different ($p < 0.0001$) than that exhibited by BTM at 84 ± 5.1 degrees (Figure 3). Representative images of draped materials are shown in Figure 3C,D. Note that the maximum possible
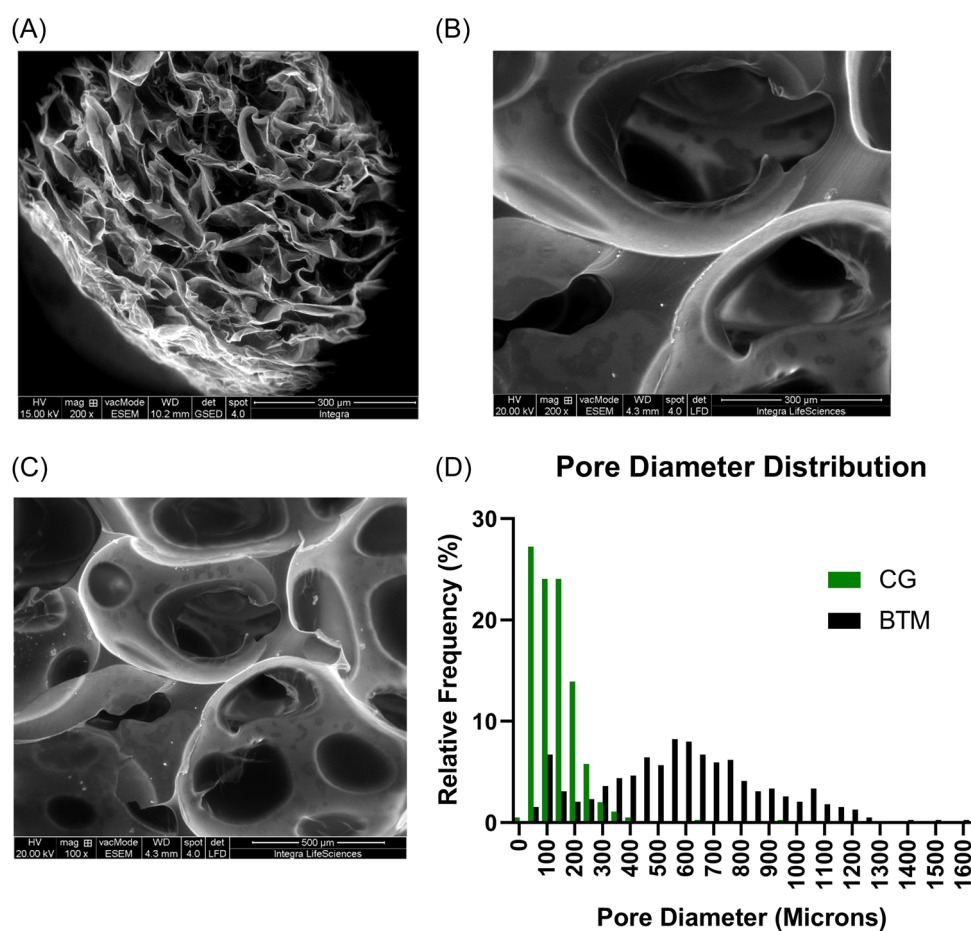

FIGURE 1 Pore size of BTM matrix is significantly larger and more diverse than that of CG matrix. Representative scanning electron micrograph images (SEM) acquired in environmental mode depict the size and layout of pores captured at ×200 magnification in (A) CG and (B) BTM, scale bar = 300 μm, as well as ×100 magnification (C) for BTM, scale bar = 500 μm. A histogram (D) depicts the distribution of pore diameters for CG (green) and BTM (black). BTM pore diameters are significantly larger than those in CG (589 vs. 132 μm averages, respectively) and more widely distributed in size. Pore measurements were captured from five and eight samples of BTM or CG, respectively, representing a minimum of 388 pores per matrix type. BTM, biodegradable temporizing matrix.
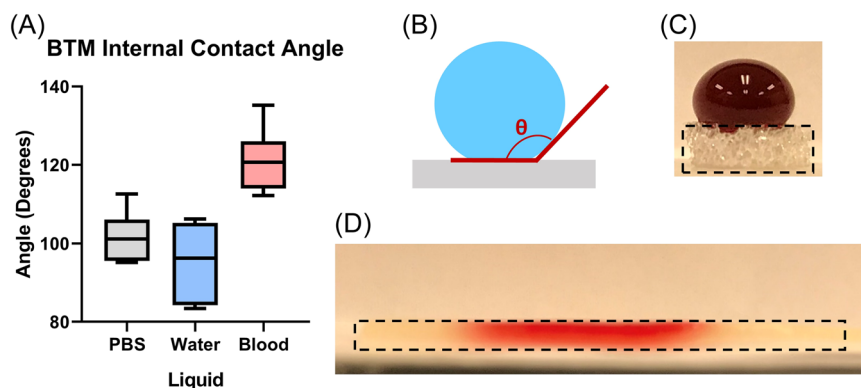
FIGURE 2 BTM exhibits hydrophobic properties whereas CG is hydrophilic. (A) Quantification of internal bending angles of varying fluid droplets placed on top of BTM angles demonstrate average values above 90 degrees, an indication of hydrophobicity. (B) A visual depiction of how internal bending angles were measured. Representative photographs of 50 μL blood droplets settled on samples of BTM (C) or CG (D), where the edges of the matrices are demarcated by a black dotted line. While blood droplets bead up on BTM, they are readily absorbed into and dispersed through the width of the CG material. Quantitation of droplet angle is not provided for CG samples because in 100% of the tests, the liquid completely absorbed inside of the matrix leaving no droplet for measurement. A total of six droplets of each liquid was tested on each matrix type. BTM, biodegradable temporizing matrix.

internal angle is 90 degrees, which would represent a completely rigid material. Since low internal bend angles align with overall material conformability, these results indicate that CG is quite conformable, whereas BTM was relatively rigid by comparison.

3.4 | Cell adhesion and proliferation

Both fibroblasts and keratinocytes demonstrated an enhanced ability to adhere to CG matrices at earlier timepoints (15 min and 2 h) compared to BTM, and overall cell numbers were significantly higher starting at 24 and 48 h for fibroblasts and keratinocytes, respectively (Figure 4A,B). The differences in cell numbers between CG and BTM matrices widen through days 3 and 4, for fibroblasts and keratinocytes, respectively, at which point overall cell numbers appear to plateau. Representative fluorescence images of the surface of fibroblast-seeded matrix constructs at day 3 confirm these findings (Figure 4C,D), showing a densely cell-covered matrix for CG compared to a sparsely populated matrix for BTM.

3.5 | Porcine wound healing study

No significant difference ($p = 0.61$) in wound contracture was observed between the CG and BTM-treated groups through day 9 postinjury, with wounds maintaining $95.1 \pm 6.0\%$ ($N = 12$) and $91.8 \pm 7.9\%$ ($N = 16$) of their original areas (9 cm^2), respectively (Figure 5A). Nontreated control wounds demonstrated significant contraction by day 7 postinjury ($75.6 \pm 9.1\%$ [$N = 4$]) and reduced further to $10.6 \pm 5.8\%$ ($N = 2$) by day 21. Histologically, both BTM and CG matrices demonstrated signs of acute inflammation with over half the granulation bed infiltrated with mononuclear cells, multinucleated giant cells (MNGCs), and, to a lesser extent, lymphocytes at day 9
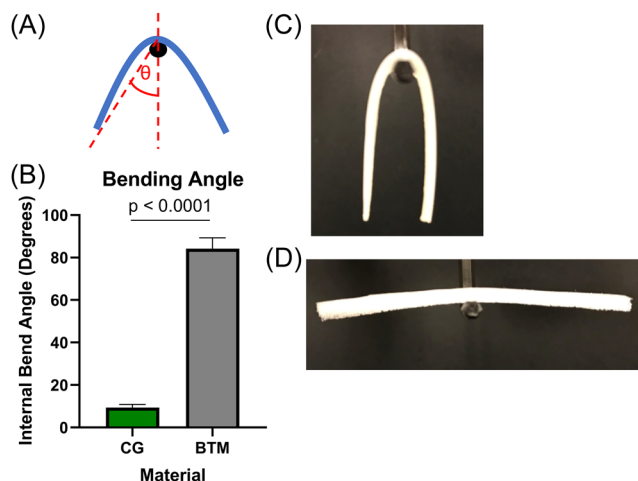

FIGURE 3 Conformability of CG is superior to that of BTM. (A) A diagram demonstrating how internal bending angles were determined within the conformability tests, with smaller angles meaning higher conformability. (B) Quantification of internal bending angles displayed as the average of three samples per matrix type. Representative images of 5 × 0.5 cm strips of matrix draped over a 3.12 mm rod are shown for (C) CG and (D) BTM matrices. All materials were prewetted for 10 min in PBS solution before getting draped over the rod matrix-side down. Statistical significance (p values) is indicated within the figure. BTM, biodegradable temporizing matrix; PBS, phosphate buffered saline.

(Figure 5B–E). Higher levels of fibroblast infiltration and fibroplasia were observed in CG matrices. While MNGCs were observed within all samples, their presence was consistently concentrated adjacent to embedded polyurethane strands in all BTM samples at both day 9 (Figure 5E) and 21 timepoints (Figure 5G). Collagen bundles in BTM-treated wounds showed early signs of organization and alignment within the microporous chambers at day 9 (Figure 5D), and these
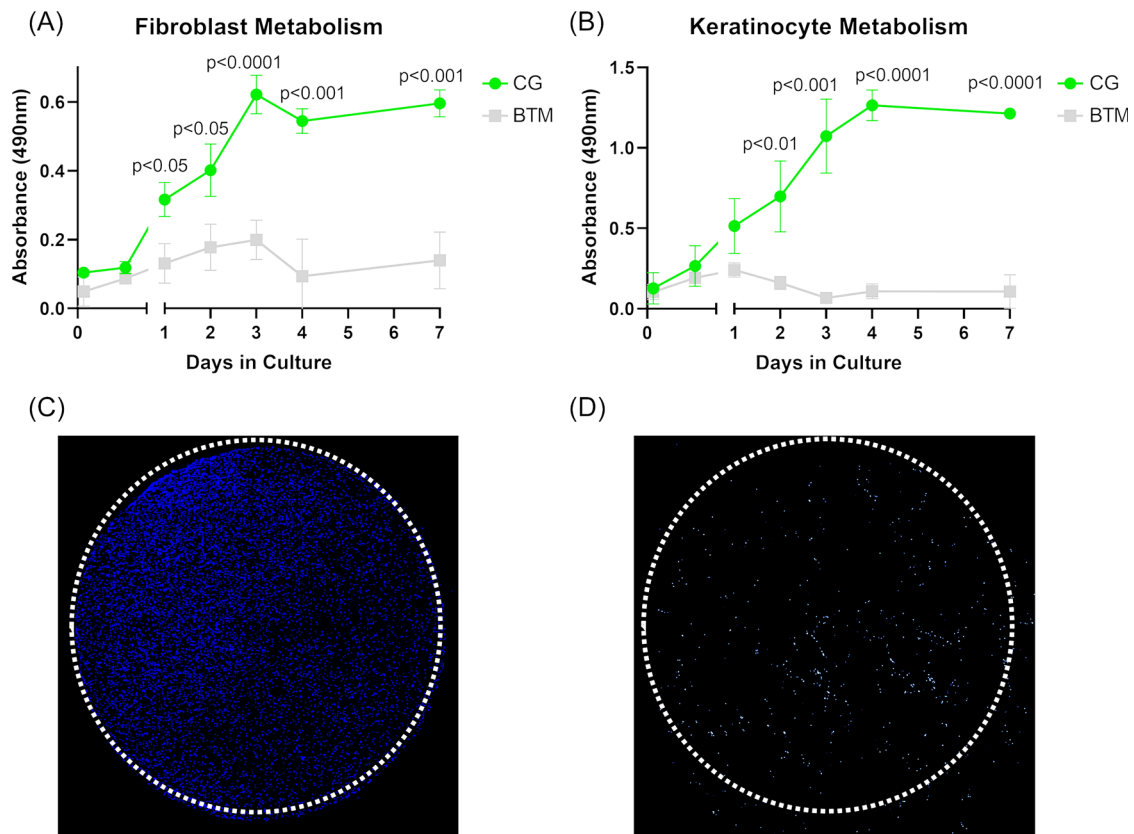
FIGURE 4 Fibroblast and keratinocyte cell adhesion and proliferation are greater on CG matrices than on BTM. Line plots depict overall (A) fibroblast and (B) keratinocyte cell metabolism (measured via MTS assay) after varying periods of incubation on the matrices. Datapoints represent three technical replicates for CG (green circles) and BTM (gray boxes) matrices. Statistically significant differences are seen as early as day 1 for fibroblasts and at day 2 for keratinocytes. Confocal fluorescent images depict the fibroblast cell coverage via DAPI stain (blue) at the surface of CG matrices (C) and BTM (D) after 3 days in culture. Matrix edges are denoted by a white dotted line for visualization. Statistical significance (p values) is indicated within the figure. BTM, biodegradable temporizing matrix; DAPI, 4',6-diamidino-2-phenylindole.
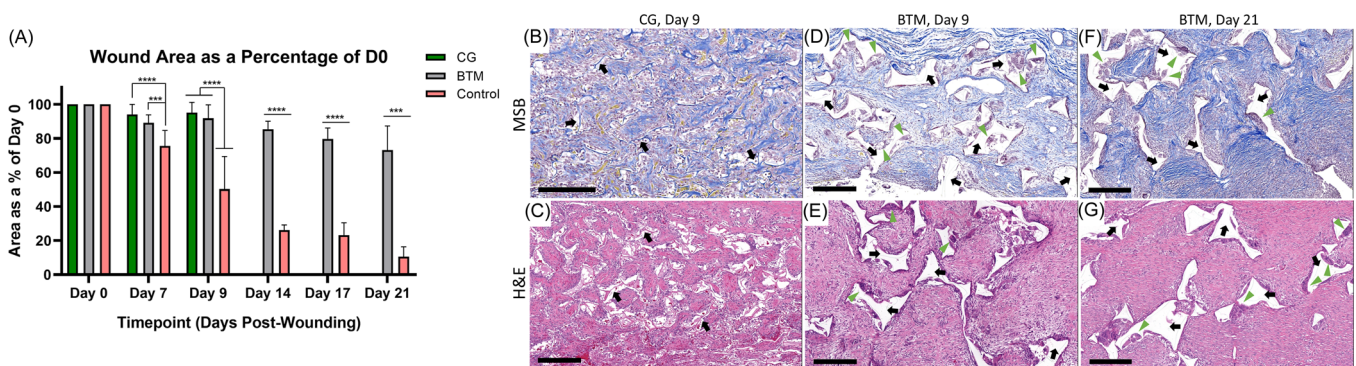

FIGURE 5 Porcine wound healing histology highlights different healing mechanisms and cellular responses to CG and BTM despite minimal macro scale contraction. (A) The bar chart depicts average wound areas over time with significant signs of contraction observed only in nontreated wounds. Representative ×5 magnification sections at 9 days postinjury for CG (B, C) and BTM (D, E) wounds demonstrate greater multinucleate giant cell (MNGC) presence and aligned collagen in BTM-treated wounds. Representative ×5 magnification images at 21 days postinjury for BTM (F, G) reveal an even greater alignment of collagen fibers within the BTM pores along with persisting MNGCs. Histology images were stained with either Martius Scarlet Blue (B, D, F) (where collagen = blue, cells = purple, and fresh fibrin = yellow) or H&E (C, E, G) (where collagen = pink and cell nuclei = dark purple). Black arrows indicate examples of residual matrix material. Green triangles indicate examples of MNGC presence. Scale bars represent either 200 μm (B) or 300 μm (C–G). BTM, biodegradable temporizing matrix.

transitioned to a marked alignment within individual microporous chambers by the 21-day timepoint (Figure 5F).

4 | DISCUSSION

This report demonstrates several fundamental physical and biological differences between the natural CG and synthetic BTM matrices. The differences seen in vivo can be corroborated to the in vitro test results.

At the macro scale, bending angle analysis (Figure 3) demonstrated clear differences in material conformability: CG was conformable whereas BTM was comparably rigid. A combination of the polyurethane's open foam architecture plus its innate stiffness likely accounts for BTM's more rigid nature. Matrix conformability influences handling characteristics and a material's ability to conform to an underlying wound bed, around joints, and other small anatomical features. Gaps or interruptions in wound contact may ultimately decrease successful engraftment of the matrix, and furthermore, can lead to void spaces underneath the sealing membrane, potentially enhancing risk of hematoma, seroma, and infection. Notably, the stiffness of the matrix fibers alone can influence how the host's body will react upon implantation. Blakney et al.[17] showed that when identical PEG-RGD hydrogels of varying stiffnesses were implanted in mice, the stiffer hydrogels were associated with increased rates of foreign body response and thicker fibrotic capsules. BTM's stiff structure may therefore partly account for the presence of aligned collagen fibers and MNGCs surrounding the embedded polyurethane fibers as visualized in histology (Figure 5).

The large differences in liquid contact angle testing may further delineate potential variations in host tissue interactions for BTM and CG relating to wettability. The in vitro results (Figure 2) suggest that CG should more readily absorb wound fluid (presumably containing immune cells, growth factors, etc.) than BTM once implanted into a wound site. This was confirmed upon visual examination of the porcine full-thickness wounds postimplantation (Figure 6). CG immediately took on a pink coloration while BTM appeared free of wound fluid except at the contact points created by the sutures. Issues with conformability and wettability with BTM may indicate the need for applied pressure to allow incorporation in the wound. However, in this study, a tri-layering bolstering scheme was used in all wounds, so this factor was not investigated.

The influence of a material's wettability also has more nuanced impacts. Hydrophobicity can influence which types of proteins are likely to adsorb, their orientation, how much they unfold or alter their 3D structures, and ultimately, which ligands proteins are able to present to cells.[18,19] Protein interactions with hydrophobic surfaces tend to result in protein denaturation that exposes hydrophobic regions to the body, and these can invoke coagulation, inflammation, and a foreign body response.[18] In the case of the serum-protein fibronectin, unfolding can activate mechanotransduction in adherent fibroblasts which may then transition to myofibroblasts and engage in
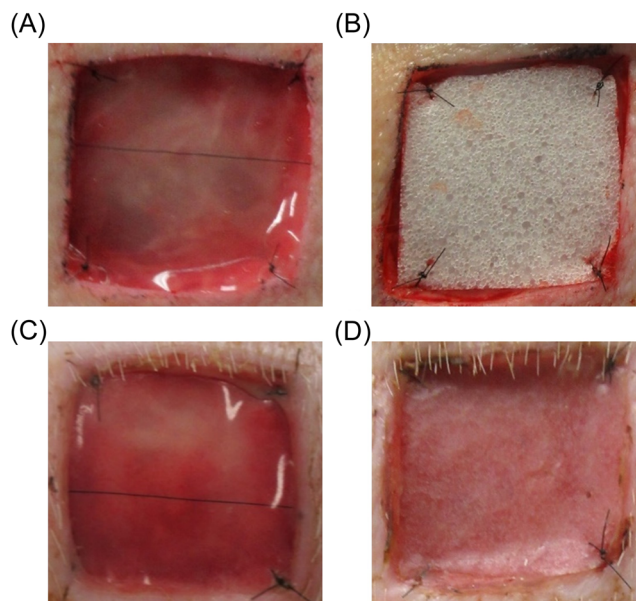

FIGURE 6 Gross appearances of treated wounds at 0 and 9 days postinjury. Top row: representative test articles in wounds immediately after being pressed into 3 × 3 cm full-thickness wounds and then sutured in place for (A) CG matrices and (B) BTM matrices. Though CG matrices are whiteish yellow before application, their quick absorption of endogenous blood results in a translucent pink appearance. BTM test articles do not as readily absorb blood and thus appear white until additional pressure is applied. Bottom row: representative test articles in wounds at 9 days postinjury for (C) CG and (D) BTM matrices, which included 7 days of a tri-layer tie-over bolster and then 2 days of a light bolster. BTM, biodegradable temporizing matrix.

fibrotic collagen deposition.[20] By comparison, mammalian cells are generally better able to adhere to hydrophilic surfaces, even in the absence of attachment ligands.[19,21] Furthermore, hydrophilic, anionic surfaces have been shown to promote apoptosis in adherent foreign body giant cells. Biomaterial-adherent macrophage apoptosis is increased by hydrophilic and anionic substrates in vivo,[22] potentially deterring a foreign body response.

Patil et al's[15] study provides valuable insight on the importance of hydrophobicity as a variable by comparing polyurethane matrices of varying engineered hydrophilicities. In a porcine excisional wound model, they found that hydrophilic polyurethane constructs, in comparison to unmodified polyurethane, exhibited improved tissue integration, lower foreign body response, higher quality granulation tissue, improved vascularization, and a more favorable immune response. The authors also compared their hydrophilic polyurethane to the exact CG and BTM matrices studied here, demonstrating that while the overall wound healing response was similar to CG, BTM exhibited inferior extracellular matrix deposition, vascularization, and immune responses.

The inherent differences in biomaterial composition between CG and BTM may explain the differing cell attachment results shown in this study. In contrast to BTM, which contains no natural cellular binding sites, CG matrices are composed of collagen and

glycosaminoglycans—both naturally-derived polymers—that possess numerous natural cell adhesion sites. Collagen contains the peptide sequences RGD, GFOGER, P15, DGEA, among others, that can be recognized by integrins, discoidin domains, and other cell surface receptors.[21] We hypothesize that these natural binding sites in combination with CG's aforementioned attributes largely contributed to the trend of increased cell attachment on CG and BTM at 15 min to 2 h in vitro (Figure 4). The subsequent increase in cell numbers in vitro on CG seen on day 1 through days 3–4 likely represents effects on cell proliferation by the matrices. Although total cell numbers appear to plateau on CG starting on days 3 and 4, this can likely be attributed to cell confluence on the matrix surface, which was confirmed through confocal imaging. By comparison, minimal cell attachment and proliferation was observed on BTM, and provision of additional time for adhesion did not improve the quality of cell interactions.

In direct contrast to our conclusions, a prior study[7] previously suggested that fibroblasts readily adhere and proliferate in vitro within this BTM material. However, there are substantial differences in key experimental factors that impact the relevancy of the findings. Most importantly, the earliest timepoint for which fibroblast adhesion data is shown is 19 days, an exceptionally long timeframe for analyzing cell adhesion, a process that typically takes place within hours. Nineteen days would be sufficient time for fibroblasts to adhere to the underlying tissue culture plastic, secrete matrix into their environment, and then subsequently migrate onto the BTM material. In our study, we purposefully made use of nontissue culture-treated plastic and subsequently moved matrices to fresh plates to avoid the cells not directly interacting with matrix articles. In alignment with our findings, the prior authors do acknowledge limited attachment of keratinocytes directly to the BTM material.

Our histological findings suggest a relationship between the enhanced cell attachment and proliferation observed in vitro and the in vivo mechanism of healing. Namely, greater amounts of fibroblast infiltration and fibroplasia were observed within CG compared to BTM by day 9 postinjury. Fibroblasts are essential to granulation tissue formation, responsible for synthesizing collagen and proteoglycans as well as remodeling local matrix environments.[23] Ample collagen was assembled within the BTM microporous chambers, presumably laid down after cells attached and migrated in on a more provisional matrix that formed therein, which was suggested as the mechanism of healing by Greenwood et al.[10]

MNGCs are present among the infiltrating cells, particularly with BTM-treated wounds where they are consistently found in close proximity to embedded residual polyurethane segments (Figure 5). MNGCs were also found within CG-treated wounds, albeit with a less distinct spatial distribution pattern. MNGCs are a normal part of the wound healing process, formed from fusion of monocytes and macrophages attempting to phagocytose tissue debris. Their numbers are often amplified, however, by presence of nondigestible matter such as that which is crosslinked, above a certain size, or of synthetic

make-up.[23] The preponderance of MNGCs surrounding BTM material is likely due to the latter two of these characteristics. Patil et al.[15] have also reported on MNGC envelopment of embedded BTM material along with dark co-localization of arginase staining, confirming cell identity. In all likelihood, this MNGC presence will be sustained following implantation, in part because BTM is known to require 18 months for full degradation, and also in light of Wagstaff et al.'s[24] human pilot study that demonstrated continual MNGC presence adjacent to polyurethane remnants a full year after implantation.

Notably, a continuous layer of MNGCs surrounding a construct, combined with aligned collagen, and hypocellularity in adjacent tissue is the hallmark of a fibrotic response or foreign body reaction. Both CG and BTM healing responses were associated with new collagen deposition aligned to some degree with residual matrix construct (Figure 5). Owing to the smaller pore size of CG, as confirmed with our pore size analysis (Figure 1), aligned collagen fibrils of a given orientation were generally limited in length by pore diameter, about 132 μm on average, resulting in an overall heterogeneous distribution of collagen orientations. By comparison, BTM matrices possessing larger pores and interconnecting void spaces allowed for greater maintenance of a collagen fibril orientation within macroporous chambers (average diameter of 589 μm) and sometimes across multiple interconnecting pores. Collagen aligned to this extent is typically associated with a fibrotic and contractile tissue response, though notably, minimal contraction of BTM-treated wounds was observed here.

Importantly, minimal contraction was observed with both CG and BTM-treated wounds. For CG, this is unsurprising given the lack of aligned collagen fibrils observed here, as well as a robust clinical literature confirming the minimal contracture and scar formation resulting from these matrices.[25] Although an earlier porcine study[4] concluded that CG matrices contract significantly more than that of BTM, these results are based on a limited sample size ($N = 1$) for CG-treated wounds. All other CG matrices from that study became prematurely delaminated due to infection, which suggests significant deficits in adherence to clinically relevant product and dressing protocols. The lack of contracture of BTM-treated wounds is likely owing to the continual presence of stiff polyurethane material throughout the wound both resisting contractile forces and providing a degree of disruption to collagen alignment.

Overall, these results show clear differences in benchtop performances between naturally-derived CG and synthetic BTM matrices, and these differences appear to influence in vivo performance. Namely, the CG matrices are hydrophilic, possess biologically meaningful pore sizes, a high degree of tissue conformity, and an ability to promote rapid cell attachment and infiltration. The lack of these qualities in BTM likely impacted the overall performance of BTM in our porcine wound model, including lower levels of fibroblast infiltration at early timepoints and the subsequent preponderance of MNGCs concomitant with aligned collagen fibrils that could indicate the early stage of a fibrotic or foreign body response. The granulation beds of CG-treated wounds appear to be in a more advanced state of

cellular infiltration by day 9 postinjury, which could translate to a shorter timeframe for readiness to graft. Indeed, clinical experience shows CG matrices are generally ready to graft about 2 weeks earlier than BTM: CG is typically ready within 14–21 days[26,27] whereas BTM usually requires 4–5 weeks.[24,28] The data presented here and data demonstrated broadly in the past 30 years of preclinical and clinical studies,[26,27,29] support the use of naturally derived skin substitute due to their potential to interact directly with host cells and proteins in the modulation of the wound healing process.

AUTHOR CONTRIBUTIONS

Victoria L Stefanelli: Conceptualization; Data curation; Formal analysis; Investigation; Methodology; Project administration; Writing—original draft. **Benjamin Mintz**: Conceptualization; Formal analysis; Investigation; Methodology. **Ankur Gandhi**: Conceptualization; Supervision; Writing—review & editing. **Jason Smith**: Supervision; Writing—original draft; Writing—review & editing.

ACKNOWLEDGMENTS

CONFLICT OF INTEREST STATEMENT

The authors of this manuscript were employed by Integra LifeSciences, which funded the entirety of the work of this manuscript, including the planning, execution, interpretation of the results, and writing the report.

DATA AVAILABILITY STATEMENT

The data that supports the findings of this study are available from the corresponding author upon a reasonable request, beginning 9 months and ending 36 months following article publication.

ETHICS STATEMENT

Bridge PTS reviewed, approved, and executed the protocol for the animal study in compliance with the US National Research Council's Guide for the Care and Use of Laboratory Animals, the US Public Health Service's Policy on Humane Care and Use of Laboratory Animals, and Guide for the Care and Use of Laboratory Animals.

TRANSPARENCY STATEMENT

The lead author Jason Smith affirms that this manuscript is an honest, accurate, and transparent account of the study being reported; that no important aspects of the study have been omitted; and that any discrepancies from the study as planned (and, if relevant, registered) have been explained.

ORCID

Jason Smith http://orcid.org/0000-0001-8381-3936

REFERENCES

1. Arenas Gómez CM, Sabin KZ, Echeverri K. Wound healing across the animal kingdom: crosstalk between the immune system and the extracellular matrix. *Dev Dyn*. 2020;249(7):834-846.
2. Varkey M, Ding J, Tredget E. Advances in skin substitutes-potential of tissue engineered skin for facilitating anti-fibrotic healing. *J Funct Biomater*. 2015;6(3):547-563.
3. Megahed MA, Elkashity SA, Talaab AA, AboShaban MS. The impact of human skin allograft as a temporary substitute for early coverage of major burn wounds on clinical outcomes and mortality. *Ann Burns Fire Disasters*. 2021;34(1):67-74.
4. Greenwood JE, Dearman BL. Comparison of a sealed, polymer foam biodegradable temporizing matrix against integra® dermal regeneration template in a porcine wound model. *J Burn Care Res*. 2012;33(1):163-173.
5. Banakh I, Cheshire P, Rahman M, et al. A comparative study of engineered dermal templates for skin wound repair in a mouse model. *Int J Mol Sci*. 2020;21(12):4508.
6. Cheshire PA, Herson MR, Cleland H, Akbarzadeh S. Artificial dermal templates: a comparative study of NovoSorb™ biodegradable temporising matrix (BTM) and Integra® dermal regeneration template (DRT). *Burns*. 2016;42(5):1088-1096.
7. Li A, Dearman BL, Crompton KE, Moore TG, Greenwood JE. Evaluation of a novel biodegradable polymer for the generation of a dermal matrix. *J Burn Care Res*. 2009;30(4):717-728.
8. Concannon E, Coghlan P, DamKat Thomas L, Solanki NS, Greenwood JE. Biodegradable temporizing matrix reconstruction of complex perineal burn wound: a case report. *J Burn Care Res*. 2021;42(5):1038-1042.
9. Greenwood JE, Schmitt BJ, Wagstaff MJD. Experience with a synthetic bilayer biodegradable temporising matrix in significant burn injury. *Burns open*. 2018;2(1):17-34.
10. Greenwood JE. A paradigm shift in practice-the benefits of early active wound temporisation rather than early skin grafting after burn eschar excision. *Anaesth Intensive Care*. 2020;48(2):93-100.
11. Bryers JD, Giachelli CM, Ratner BD. Engineering biomaterials to integrate and heal: the biocompatibility paradigm shifts. *Biotechnol Bioeng*. 2012;109(8):1898-1911.
12. Sadtler K, Wolf MT, Ganguly S, et al. Divergent immune responses to synthetic and biological scaffolds. *Biomaterials*. 2019;192:405-415.
13. Brown BN, Barnes CA, Kasick RT, et al. Surface characterization of extracellular matrix scaffolds. *Biomaterials*. 2010;31(3):428-437. doi:10.1016/j.biomaterials.2009.09.061
14. Lu Y, Aimetti AA, Langer R, Gu Z. Bioresponsive materials. *Nature Reviews Materials*. 2016;2(1):16075.
15. Patil P, Russo KA, McCune JT, et al. Reactive oxygen species–degradable polythioketal urethane foam dressings to promote porcine skin wound repair. *Sci Transl Med*. 2022;14(641):eabm6586. https://www.science.org/doi/10.1126/scitranslmed.abm6586
16. Dearman BL, Li A, Greenwood JE. Optimization of a polyurethane dermal matrix and experience with a polymer-based cultured composite skin. *J Burn Care Res*. 2014;35(5):437-448.
17. Blakney AK, Swartzlander MD, Bryant SJ. Student award winner in the undergraduate category for the society of biomaterials 9th world biomaterials Congress, Chengdu, China, June 1-5, 2012: the effects of substrate stiffness on the in vitro activation of macrophages and in vivo host response to poly(ethylene glycol)-based hydrogels. *J Biomed Mater Res A*. 2012;100(6):1375-1386.
18. Sheikh Z, Brooks P, Barzilay O, Fine N, Glogauer M. Macrophages, foreign body giant cells and their response to implantable. *Materials*. 2015;8(9):5671-5701.
19. Sridharan R, Cameron AR, Kelly DJ, Kearney CJ, O'Brien FJ. Biomaterial based modulation of macrophage polarization: a review and suggested design principles. *Mater Today*. 2015;18(6):313-325.

20. Cao L, Nicosia J, Larouche J, et al. Detection of an integrin-binding Mechanoswitch within fibronectin during tissue formation and fibrosis. *ACS Nano*. 2017;11(7):7110-7117.

21. Anselme K, Ploux L, Ponche A. Cell/material interfaces: influence of surface chemistry and surface topography on cell adhesion. *J Adhes Sci Technol*. 2010;24(5):831-852.

22. Brodbeck WG, Patel J, Voskerician G, et al. Biomaterial adherent macrophage apoptosis is increased by hydrophilic and anionic substrates in vivo. *Proc Natl Acad Sci USA*. 2002;99(16): 10287-10292.

23. Anderson JM, McNally AK. Biocompatibility of implants: lymphocyte/macrophage interactions. *Semin Immunopathol*. 2011;33(3): 221-233.

24. Wagstaff MJ, Schmitt BJ, Coghlan P, Finkemeyer JP, Caplash Y, Greenwood JE. A biodegradable polyurethane dermal matrix in reconstruction of free flap donor sites: a pilot study. *Eplasty*. 2015;15:13.

25. Yannas IV, Burke JF. Design of an artificial skin. I. Basic design principles. *J Biomed Mater Res*. 1980;14(3):339.

26. Branski LK, Herndon DN, Pereira C, et al. Longitudinal assessment of Integra in primary burn management: a randomized pediatric clinical trial. *Crit Care Med*. 2007;35(11):2615-2623.

27. Heimbach DM, Warden GD, Luterman A, et al. Multicenter postapproval clinical trial of Integra® Dermal Regeneration Template for burn treatment. *J Burn Care Rehabil*. 2003;24(1):42-48.

28. Larson KW, Austin CL, Thompson SJ. Treatment of a Full-Thickness burn injury with NovoSorb biodegradable temporizing matrix and RECELL autologous skin cell suspension. *J Burn Care Res*. 2020;41(1): 215-219.

29. Prezzavento GE, Calvi RNJ, Rodriguez JA, Taupin P. Integra dermal regeneration template in reconstructive surgery for cutaneous tumours: a two-year retrospective review. *J Wound Care*. 2022;31(7):612-619.